Chapter 1

Introduction

Twenty years have passed since the discovery of the first copper-oxide high-temperature superconductor $La_{2-x}Ba_xCuO_4$ in 1986, and the intriguing physics of cuprate superconductors continues to fascinate scientists. Coherent comprehension of the underlying mechanism remains elusive. Nevertheless, a number of superconducting and normal-state properties are now understood in great detail from the comparison of experimental findings to theoretical analyses of simple models. In this chapter, we review the basic properties of the cuprate superconductors, survey the current experimental and theoretical progress, and conclude with a brief outline of the thesis.

1.1 Crystalline structures and electronic phase diagram of high-temperature superconductors

1.1.1 Crystalline and electronic structures of parent compounds

Cuprate superconductors are generally referred to as doped Mott insulators. To understand the origin of this terminology, we begin with an investigation of the cuprate crystalline and electronic structures. All high T_c superconductors share the following two elements: the CuO_2 planes that form single-layer or multilayer conducting blocks per unit cell, and the "charge reservoirs" in between the CuO_2 planes that are responsible for contributing either electrons or holes to the CuO_2 planes. In Fig. 1.1, three representative cuprate superconductors, the one-layer hole-doped $La_{2-x}Sr_xCuO_4$ (LSCO), the one-layer electron-doped $Nd_{2-x}Ce_xCuO_{4\pm\delta}$ (NCCO), and the infinite-

layer $Sr_{1-x}La_xCuO_2$ (SLCO), are illustrated as examples. It is understood that the electronic states of the CuO_2 planes control the physics of high T_c superconductivity. By doping with substitution elements or by changing the oxygen content (as in $YBa_2Cu_3O_{6+\delta}$) in the charge reservoirs, the carrier density in the CuO_2 planes can be controlled.

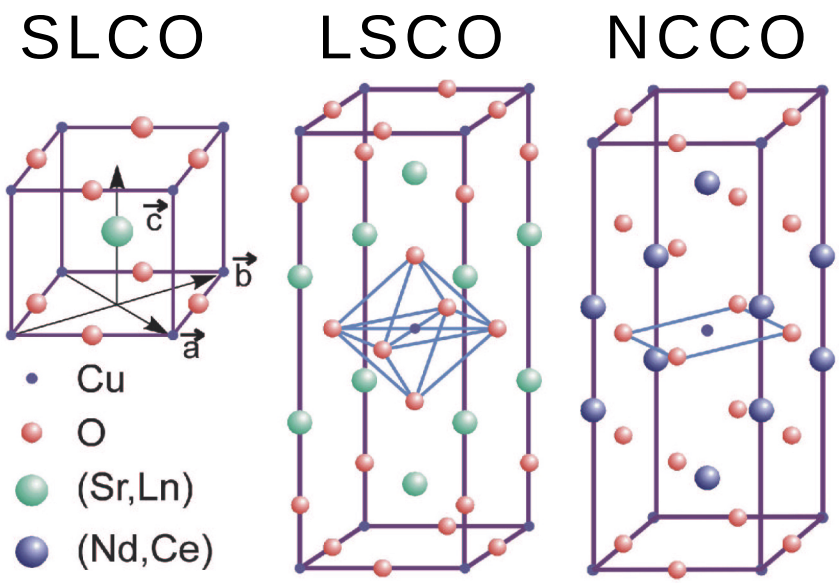

Figure 1.1: Crystalline structures of representative hole-doped and electron-doped cuprates: electron-doped $Sr_{1-x}La_xCuO_2$ (SLCO), hole-doped $La_{2-x}Sr_xCuO_4$ (LSCO), and electron-doped $Nd_{2-x}Ce_xCuO_{4\pm\delta}$ (NCCO). We note the absence of apical oxygen in all electron-doped cuprates, in contrast to the presence of CuO_6 octahedron in hole-doped cuprates. Furthermore the infinite-layer system differs from all others in that no excess charge reservoir exists between consecutive CuO_2 planes.

In the undoped parent compound, the electronic states of the Cu on the plane are in the d^9 configuration. The presence of oxygen octahedron sounding the central Cu ion and the associated Jahn-Teller distortion split the degenerate e_g orbitals of Cu d^9 with the resulting highest partially occupied orbital being $d_{x^2-y^2}$. The Cu $d_{x^2-y^2}$-orbital and the doubly occupied O p_x, p_y-orbitals form a strong covalent bonding. In the absence of interaction among electrons, the hybridization of these three orbitals gives rise to the bonding, non-bonding and half-filled anti-bonding bands and predicts a good metal, in sharp contrast to the large charge gap observed in the undoped compounds.

The failure of the band theory, and hence that of the conventional Fermi liquid approach to high T_c problems, stems from the existence of a large on-site Coulomb interaction that well exceeds the bandwidth of the tight-binding anti-bonding band. If a charge carrier were to hop onto a partially

filled Cu $d_{x^2-y^2}$ orbital, the two Cu $d_{x^2-y^2}$ carriers would experience a large energy penalty, and, hence, it is energetically more favorable to localize the electrons. Electronic systems with half-filled states and strong localizations are known as Mott insulators. Specifically, the strong on-site Coulomb repulsion suppresses charge fluctuations, splits the half-filled anti-bonding band into an empty upper-Hubbard band and a filled lower-Hubbard band, thereby turning a band metal into a Mott insulator with an optical gap of a few eV.

More precisely, in the cuprate systems, the energy penalty of having a second hole in the Cu d-orbital is much larger than the energy separation between the Cu $d_{x^2-y^2}$ and O p-orbitals. Thus, the extra hole primarily goes to the O p_x, p_y orbitals, and the energy cost $(E_p - E_d)$, of the order of $\sim 2\ eV$, is named the charge transfer gap. Because the hybridization integral, t_{dp}, is much smaller than the energy barrier $(E_p - E_d)$, the electrons in the undoped compounds form localized moments on the Cu sites. These spins are anti-ferromagnetically aligned via the super-exchange interaction that involves virtual hopping to the neighboring O p-orbitals. As a result, the parent compounds of high T_c materials are referred to as anti-ferromagnetic Mott insulators.

1.1.2 Electronic phase diagrams

When charge carriers are introduced to the CuO_2 planes, several novel phases appear as exemplified in Fig. 1.2. This section provides an overview of the electronic phase diagrams of cuprates and summarizes the most important phenomena shared among all cuprate superconductors. We remark that the physics of cuprate superconductors is extremely rich, and therefore a simplified phase diagram such as that shown in Fig. 1.2 cannot capture many interesting details that take place in different cuprate systems. Since the physics behind these non-universal phenomena is the main theme of the thesis, we shall discuss these issues in more detail later in this chapter [§1.2].

As mentioned in the previous section, at zero doping, the electronic state of the parent compound is an anti-ferromagnetic Mott insulating state for both the n-type (electron-doped) and the p-type (hole-doped) cuprates. Chronologically, soon after the discovery of La_2CuO_4, long-range Néel spin ordering in this system was experimentally determined [1]. Strictly speaking however,

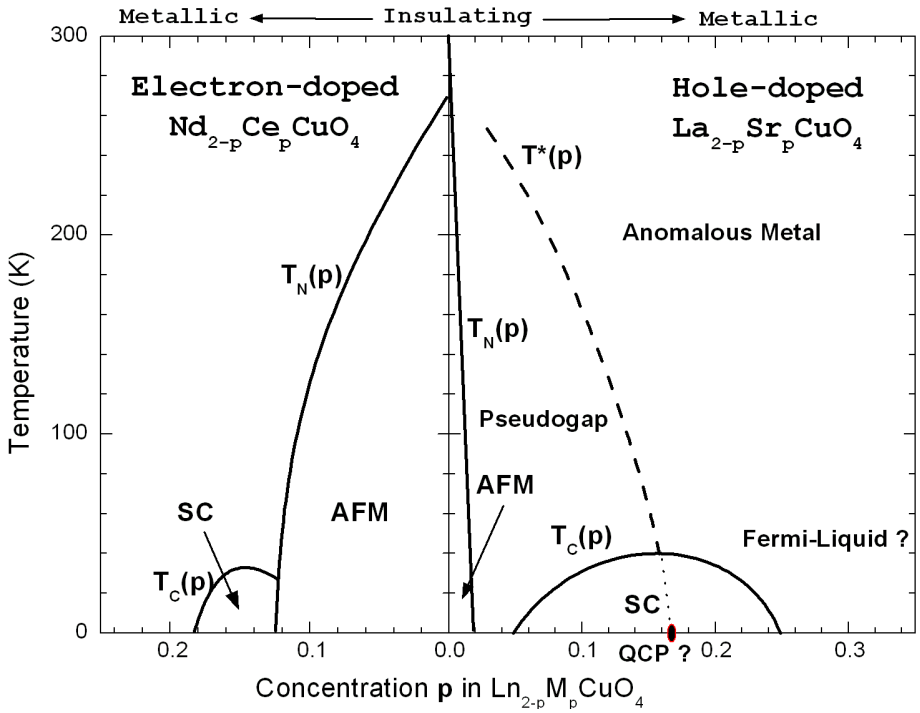

Figure 1.2: The zero-field temperature (T) vs. doping (x) phase diagram of representative electron-doped (n-type) and hole-doped (p-type) cuprate superconductors. AFM: long-range commensurate anti-ferromagnetic order. SC: superconducting state. PG: pseudogap region. FL: Fermi liquid. T_N, T_c, and T^* are respectively the Néel temperature, the superconducting transition temperature, and pseudogap temperature.

the Hohenberg-Mermin-Wagner theorem asserts that an ideal two-dimensional (2D) magnetic system with isotropic anti-ferromagnetic Heisenberg couplings would remain magnetically disordered at finite temperature. The finding of long-range anti-ferromagnetic ordering in real systems can be reconciled with theory by relaxing the strict 2D picture and incorporating three-dimensional (3D) anisotropic effects. The anisotropic effects in cuprate can arise through many different ways. For instance, in addition to the dominant 2D Heisenberg term, there are small interlayer coupling, Dzyaloshinski-Moriya (DM) anisotropic coupling and easy-plane (x-y) anisotropic coupling terms in the real and spin space Hamiltonian [2]. In orthorhombic systems, such as La_2CuO_4, DM and interlayer anisotropies stabilize the 3D long-range anti-ferromagnetic phase [3, 4]. In tetragonal systems, such as Nd_2CuO_4, where the former two anisotropies are absent, x-y anisotropy results in a crossover from the 2D Heisenberg behavior to the 2D XY regime, followed by a crossover to the 3D XY regime, and hence stabilizes the long-range Néel order [5, 4].

As holes are introduced to the CuO_2 planes, the Néel temperature of the system decreases rapidly upon doping and the commensurate anti-ferromagnetic (AFM) long-range order disappears completely at around $p \sim 0.02$, where p is the number of doped holes per Cu. Above this doping level, various types of spin fluctuations replace the original commensurate AFM order and continue to survive in the superconducting phase. In $La_{2-x}Sr_xCuO_4$ ($x = p$ for the one-layer systems), static incommensurate spin fluctuations develop beyond the Néel state and persist in the superconducting state, while in other compounds, such as $YBa_2Cu_3O_{6+\delta}$, commensurate magnetic resonance modes and significant dynamic spin fluctuations coexist with superconductivity in the underdoped and optimally doped region.

When hole-doping is further increased, superconductivity sets in at $p \sim 0.05$ and lasts up to $p \sim 0.25$. There is general consensus that the pairing symmetry of the superconducting order parameter of hole-doped cuprates is predominantly $d_{x^2-y^2}$-like in the underdoped and optimally doped[1] region [6, 7]. In the heavily overdoped limit, on the other hand, a significant s-wave component in addition to the $d_{x^2-y^2}$ component has been revealed [8] [§1.2.1].

In the normal state of the underdoped cuprates, various phenomena associated with a partially suppressed density of states around the Fermi level and an opening of the spectral gap in the spin and charge fluctuations have been observed [9]. This state is termed as the pseudogap phase [§1.2.2]. Near the optimal doping, the pseudogap phase crosses over to an anomalous non-Fermi-liquid region where quantum critical scaling behavior in the spin and charge density fluctuations is suggested [10, 11]. As we further increase the doping to the overdoped range, conventional Fermi-liquid physics is eventually recovered.

On the electron-doping side, despite an overall similarity, we notice that the AFM state exists over a wider doping range and the superconducting region is much narrower in comparison with that of the hole-doped cuprates. An intuitive way to visualize the robustness of the AFM order in the electron-doping phase diagram is the spin-dilution picture. While the hole doping introduces carriers to the O p-orbitals, the electron doping takes place in the Cu d-orbital. The resulting mobile spinless

[1] The optimal doping $p_0 \approx 0.16$ is defined as the doping concentration with the highest transition temperature $T_c(p_0)$. Underdoping refers to the doping level where $p < p_0$, and overdoping refers to $p > p_0$.

Cu $3d^{10}$ configuration dilutes the background anti-ferromagnetic coupling and leads to a gradual reduction of the Nèel temperature [12]. The suppression of T_N is comparable to that observed in the Zn-doped La_2CuO_4 [13, 14] where the doped Zn with a localized $3d^{10}$ configuration dilutes the AFM order of the Cu spins. In contrast, the doped holes in the O orbitals induce ferromagnetic coupling between adjacent Cu spins, strongly frustrating the anti-ferromagnetic background [15]. Therefore, the Néel temperature drops rapidly with increasing hole doping, and the resulting AFM phase is much narrower in the hole-doped cuprates.

In the normal state of the n-type cuprates, no discernible zero-field low-energy pseudogap is observed by the tunneling and photoemission spectroscopy measurements, although, upon the application of a large magnetic field that fully suppresses superconductivity, a partial tunneling gap is again detected [16, 17, 18] [§1.2.2]. Besides, the electronic properties of the normal state measured by the transport and zero-field tunneling experiments are more conventional, similar to what the Fermi-liquid region in the overdoped p-type cuprates exhibits.

1.1.3 Effective single-band Hubbard model and $t - J$ model

The electronic states responsible for the essential physics in cuprate superconductors are the Cu $d_{x^2-y^2}$ orbital and the O p_x, p_y orbitals. Therefore, to understand the generic features of the cuprate phase diagram, a sensible starting point may be a three-band Hubbard model [19], which includes both the Cu and O orbitals. However, there is strong evidence that the single-band Hubbard model suffices to account for many important aspects of cuprate physics [20], even though it is not apparent why one could safely ignore the oxygen orbitals when constructing a low-energy Hamiltonian. This issue was addressed by the insight of Zhang and Rice [21], which brings forward the importance of the singlet formation between the doped O hole and the Cu hole originally residing at the half-filled central Cu^{2+} ions [Fig. 1.3]. It is by considering the low-energy theory of the singlet motion in the CuO_2 planes that we arrive at an effective single-band model proposed by Anderson [20].

In the hole-doped cuprates, the primary driving force of the singlet formation is the reduction in kinetic energy from phase coherence and from Cu − O hybridization. According to the second-

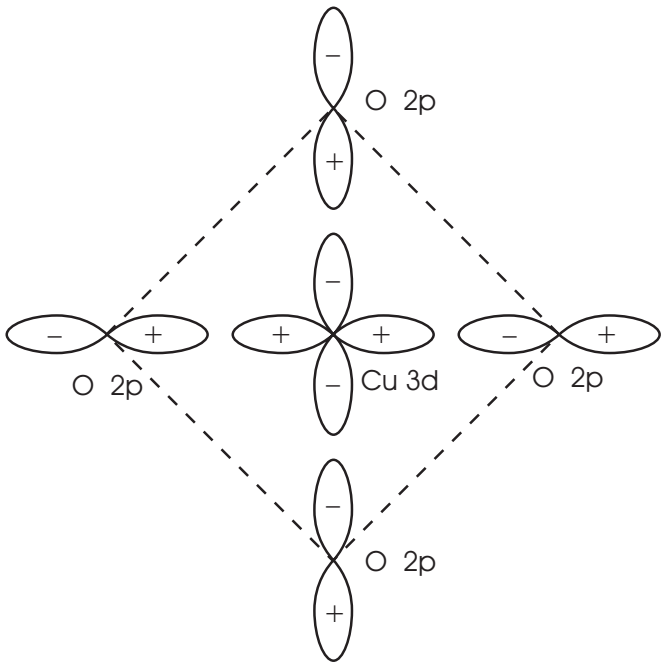

Figure 1.3: Schematic diagram of a single CuO_4 cluster and the hybridization of the Cu $3d^9$ hole with the surrounding O $2p$ hole states.

order perturbation calculation [21], to maximize the energy gain, a doped hole first spreads out as a symmetric coherent superposition of the four O $2p$ hole states surrounding the Cu^{2+} ion and then hybridizes with the central Cu $d_{x^2-y^2}$ hole to form a Zhang-Rice singlet [Fig. 1.3]. Since the symmetric O hole states localized at different CuO_4 clusters are not orthogonal, a proper set of Wannier functions for the whole lattice has to be constructed from the localized states. By hybridizing the symmetric O Wannier states with the central Cu $d_{x^2-y^2}$ states, the original three-band Hamiltonian can be rewritten in terms of this new basis.

The resulting low-energy effective Hamiltonian of the Zhang-Rice singlets in the CuO_2 plane reduces to a single-band Hubbard model, which contains an effective singlet hopping matrix element $t_{i,j,\sigma}$ and an effective potential term $U \sim (E_d - E_p)$ where E_d (E_p) is the energy of the Cu $d_{x^2-y^2}$ (O $2p_x, 2p_y$) holes,

$$H = -\sum_{<i,j>,\sigma} \Big[t_{i,j,\sigma} c^{\dagger}_{i,\sigma} c_{j,\sigma} + h.c. \Big] + \sum_{i,\sigma} U n_{i,\sigma} n_{i,\sigma}. \tag{1.1}$$

In Eq. (1.1), i and j label the lattice sites, and the first summation is over the nearest neighbors.

In the high U (strong-coupling) limit, Hubbard model is reduced to the $t-J$ model:

$$H = P\left(-\sum_{<i,j>,\sigma}\left[t_{i,j,\sigma}c^{\dagger}_{i,\sigma}c_{j,\sigma}+h.c.\right]+J\sum_{<i,j>}\left[(\vec{S_i}\cdot\vec{S_j}-\frac{1}{2}n_in_j\right]\right)P, \tag{1.2}$$

where the exchange coupling is given by $J = 4t^2/U$, and P is the projection operator that projects out the double occupancy states. For the electron-doped cuprates, mapping from the three-band model to the one-band Hubbard model is more apparent because the doped charge carriers, instead of going to the O sites, fill up the Cu $3d$-orbitals. By replacing the hybridization hopping t_{pd} with a second-order effective hopping element and assuming that U is large, we arrive at exactly the same single-band $t-J$ model (1.2). In this case, the effective Hamiltonian characterizes the hopping of the Cu $3d^{10}$ configuration, in contrast to that of the Zhang-Rice singlets for hole doping.

We note that, although in the lowest-order approximation the three-band Hubbard model reduces to the single-band $t-J$ model for both electron- and hole-doped cuprates, this theory cannot account for the asymmetry in the phase diagram between the two types of cuprates [Fig. 1.2] because the one-band $t-J$ model with nearest-neighbor hopping is electron-hole symmetric. Introducing further neighbor couplings into the one-band model could break the symmetry [22, 23, 24]. However, when solved on finite clusters, the three-band Hubbard model with parameters derived from the *ab initio* local density functional theory generates similar nearest-neighbor t and next-nearest-neighbor t' hopping elements in the effective model for both types of doping [25]. This difficulty can be circumvented if an additional Cu $4s$ orbital is taken into account [26]. It is known that the apical oxygens in the hole-doped cuprates modulate the Cu $4s$ orbital [27] and thus change the t'/t ratio significantly. Since electron-doped cuprates have no apical oxygen atoms, it may explain why they have a different t'/t value and thus a disparate phase diagram from that of the hole-doped cuprates. At the time of writing, we do not know what the suitable microscopic model is for electron-doped cuprates. More theoretical effort is necessary to better elucidate the *microscopic* origin of the asymmetry in the phase diagram.

1.2 Electron-doped vs. hole-doped cuprates: review of current experimental and theoretical status

As a first-order description, the one-band Hubbard model and its derivative $t-J$ model capture the essential physics of the doped anti-ferromagnetic Mott insulators, *i.e.*, the competition between the kinetic energy (t) that favors the delocalization of charge carriers and the anti-ferromagnetic exchange interaction (J) originated from the strong on-site Coulomb repulsion. Mean field theory of the $t-J$ model supplemented by an off-site Coulomb potential reveals a plethora of possible ground states closely spaced in energy [28], characterized by their respective broken symmetries and their distinctive low-energy excitations. A central objective of the high T_c research is to determine which orders are responsible for the cuprate phenomenology. In this section, we review the experimental findings that uncover the competing gound states and comment on related theoretical proposals advocating for specific orders. We focus on contrasting the pairing symmetry and the pseudogap phenomena between the electron- and hole-doped cuprates and discuss how these apparent non-universal phenomena are linked to the presence of competing orders.

1.2.1 Pairing symmetry

The identification of the pairing symmetry is an important step toward determining the pairing mechanism of high-temperature superconductivity because it poses great constraints on the microscopic theory. Empirically, the Knight shift and spin-lattice relaxation measurements by the nuclear magnetic resonance (NMR) technique have shown that carriers in cuprate superconductors form singlet pairing below the transition temperature [29, 30]. Consequently, from a symmetry consideration the parity of the (orbital) order parameter must be even. In a quasi-two-dimensional system where interlayer coupling is sufficiently weak and electron motion is strongly confined in the CuO_2 planes, d-wave pairing is preferable because it minimizes the on-site Coulomb repulsion while retaining 2D confinement. When the interlayer coupling strength increases, however, s-wave pairing becomes more favorable as the system gains a larger condensation energy at the expense of the Coulomb

energy.

It is well established that the pairing symmetry of the underdoped and optimally doped p-type cuprates is predominately d-wave [6, 7] [Fig. 1.4(a)]. Preponderant evidence from non-phase-sensitive experiments such as the angular-resolved photoemission spectroscopy (ARPES) [31], thermal conductivity [32], and penetration depth measurements [33] has revealed the anisotropy of the pairing potential, the presence of line nodes, and the existence of low-energy nodal quasiparticles. Additionally, ingenious phase-sensitive techniques such as the SQUID interferometry [34], single-Josephson-junction modulation [34, 35], and tricrystal scanning SQUID magnetometry [36] experiments have confirmed the change of phase across the line nodes, which is consistent with a d-pairing symmetry.

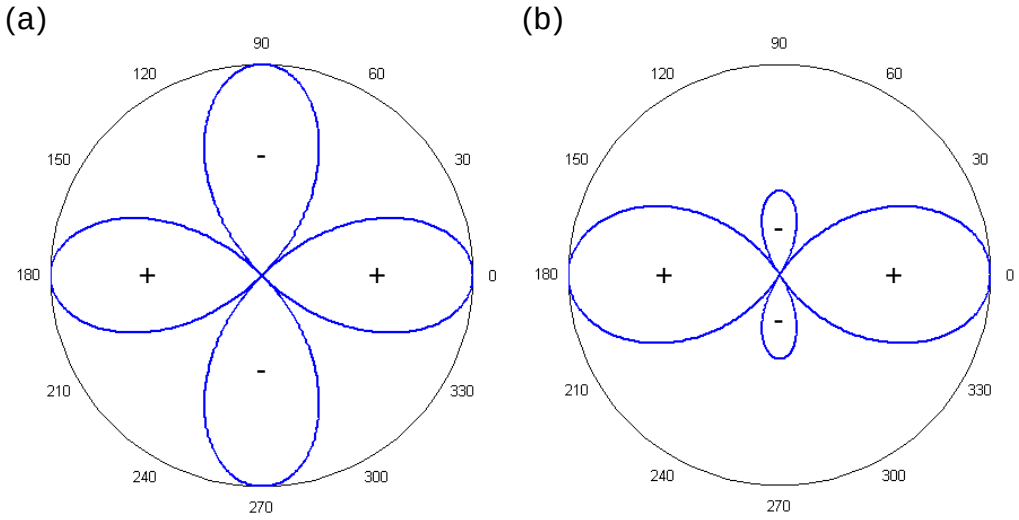

Figure 1.4: Magnitude and phase of the superconducting order parameter as a function of direction in the momentum space. The superconducting order parameter of (a) a d-wave superconductor is given by $\Delta_d(\mathbf{k}) = \Delta \cos 2\theta_{\mathbf{k}}$, where Δ is the maximum gap value and $\theta_{\mathbf{k}}$ is the angle between the quasiparticle wavevector $\mathbf{k}$ and the antinode direction, while that of (b) a $(d+s)$-wave superconductor is $\Delta_{(d+s)}(\mathbf{k}) = \Delta\left[(1-x)\cos 2\theta_{\mathbf{k}} + x\right]$. In figure (b), $x = 30\%$ s-wave admixture is assumed.

Curiously, in the heavily overdoped cuprates, there is a significant s-wave component mixing into the d-wave order parameter [Fig. 1.4(b)]. Our tunneling results on the overdoped $(Y_{0.7}Ca_{0.3})Ba_2Cu_3O_{6+\delta}$ (Ca-YBCO, doping level $p \approx 0.22$) thin films [8] find a substantial Δ_s/Δ_d ratio [§4], where Δ_s and Δ_d are the magnitudes of the s-wave and d-wave components. Subsequent ARPES measurements on overdoped $YBa_2Cu_3O_{6.993}$ (YBCO) ($p \approx 0.18$) reconfirms the large in-plane gap anisotropy [37]. In addition, Raman spectroscopy results on tetragonal $Bi_2Sr_2CaCu_2O_{8+\delta}$ (Bi-

2212) [38] and $Tl_2Ba_2CuO_{6+\delta}$ (Tl-2201) [39] single crystals suggest that the s-wave mixing with overdoping is a generic feature of high T_c superconductors regardless of the crystalline symmetry.

In the electron-doped cuprates, the determination of the pairing symmetry has been more controversial. While quasiparticle tunneling spectroscopy [40, 41] and earlier Raman spectroscopy [42] indicate an s-wave pairing in nearly optimally doped one-layer $Nd_{2-x}Ce_xCuO_{4-\delta}$ (NCCO) and $Pr_{2-x}Ce_xCuO_{4-\delta}$ (PCCO), tricrystal SQUID magnetometry [43], ARPES measurements [44, 45], and recent Raman spectroscopy results [46] are more consistent with d-wave pairing.[2] Recently, doping-dependent pairing symmetry is observed by point-contact spectroscopy [47] and penetration depth measurements [48], where the change from d-wave pairing in the underdoped to s-wave in the optimally doped and overdoped one-layer PCCO is reported. Furthermore, scanning tunneling spectroscopy studies of the infinite-layer $Sr_{0.9}La_{0.1}CuO_2$ (SLCO) [49] have identified an s-wave pairing [§5] in this simplest cuprate compound that is free of the complications from the $Cu-O$ chain effect as in YBCO and the oxygen inhomogeneity induced disorder as in NCCO, PCCO, and Bi-2212.

The non-universal pairing symmetry observed in electron-doped and hole-doped cuprates indicates that, instead of being a ubiquitous property of high-temperature superconductors, the symmetry of the order parameter varies with material-dependent properties including the anisotropy ratio, the on-site Coulomb repulsion and the anti-ferromagnetic coupling strength. Thus, the pairing symmetry is possibly a mere consequence of the compromise between different competing energy scales [50] rather than a sufficient condition of cuprate superconductivity.

1.2.2 Pseudogap

The first experiments showing evidence for a normal state gap-like feature in the hole-doped cuprates are the temperature-dependent NMR spin-lattice relaxation rate and Knight shift measurements of underdoped YBCO [51, 52]. The spectral weight of the low-frequency spin fluctuations is transferred to the high-frequency range in the normal state, and a "spin gap" is developed well above

[2] We note that the d-wave pairing observed in ARPES [45] and Raman scattering [46] is not an exact $d_{x^2-y^2}$ symmetry, since the maximum gap is displaced away from the $[\pi, 0]$ to where the Fermi surface crosses the magnetic Brillouin zone boundary, indicating a strong coupling to the background anti-ferromagnetic fluctuations in the one-layer electron-doped cuprates.

the transition temperature T_c. Other measurements probing the charge, spin, and single-particle excitations of underdoped p-type cuprates all hint at an opening of low-energy spectral gaps above T_c. The development of spectral gaps in spin fluctuations (as measured by the NMR spin-lattice relaxation rate), in charge fluctuations (as measured by the optical conductivity spectra via infrared reflectance [53]), and in single-particle excitation spectra (as measured by the tunneling spectroscopy [54] and ARPES [55, 56]) all takes place at different temperatures. In the phase diagram given by Fig. 1.2, we define the pseudogap temperature $T^*(p)$ as the temperature below which a suppression of electronic density of states around the Fermi level develops.

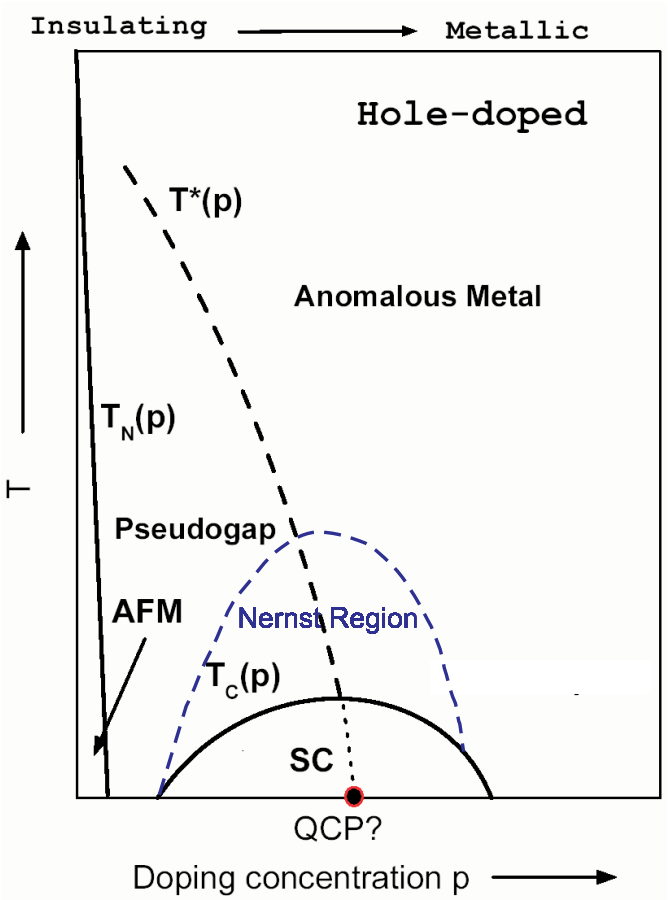

Figure 1.5: Schematic phase diagram for the hole-doped cuprates showing that the Nernst region only covers a small part of the pseudogap phase. Note that the "normal" metal coincides with the anomalous metal state shown in Fig. 1.2.

While NMR, neutron scattering, transport, and optical conductivity measurements probe the reduced spin and charge scattering rates, tunneling spectroscopy and ARPES probe directly the

loss of single-particle density of states. ARPES measurements of underdoped Bi-2212 reveal a normal state (leading edge) spectral gap whose magnitude and momentum anisotropy resembles the superconducting gap [55, 56], and the earlier tunneling spectroscopy measurements observe a smooth evolution of the superconducting gap into the pseudogap [57, 54]. Based on these results, some physicists speculate that the pseudogap is a precursor to the superconducting gap.

There are two main categories of theories under the precursor scenario: the "pre-formed magnetic pairing" conjecture and the "pre-formed Cooper pairing" conjecture. Representative theories of pre-formed magnetic pairs include the resonating valence bond (RVB) theory and its derivative, the $SU(2)$ gauge theory [20, 58], which view the pseudogap as a spin gap opening up upon the singlet pairing below a pseudogap temperature T^*. In the theory, the singlet pairing fluctuates and resonates among different pairs, thus restoring translational symmetry of the CuO_2 planes. This ground state is known as an RVB spin liquid state. The orbital wavefunction of such a pseudogap phase could display staggered-flux correlations [58, 59], equivalent to the d-wave superconducting correlations in the zero-doping limit [60]. By cooling the pre-formed magnetic-pair system below T_c, the singlet pairs would turn into Cooper pairs, so that long-range superconductivity becomes established. Experimental data suggestive of this scenario have been reported by the observation of a normal state spin gap in NMR measurements [61]. However, direct observation of the proposed staggered flux phase (in which orbital currents circulate in a staggered pattern) remains elusive. Furthermore, that there is no apparent broken symmetry in an RVB spin liquid cannot be easily reconciled with numerous experimental reports on the observation of broken symmetries in cuprates [§1.2.3]. Another version of the pre-formed magnetic pairing scenario suggests that the singlet pairing would result in a valence-bond solid (spin-Peierls state) instead of the RVB spin liquid [62]. At low temperatures, the conjecture of the bond-ordered states seems to be consistent with several experimental phenomena. However, a finite-temperature theory directly applicable to the pseudogap phase is still lacking.

In the preformed Cooper pair scenario, the pseudogap phase is regarded as a state with strong superconducting phase fluctuations resulting from the small phase stiffness in high T_c cuprates [63].

The pairing potential in the pseudogap phase is non-vanishing, and hence the spectral gap is non-zero, though the phase coherence is lost. The supporting experimental evidence for the fluctuating superconducting order above T_c is provided by the Nernst experiments, where the short-range superconducting correlations are manifested as the non-zero Nernst signals [64, 65, 66]. However, the Nernst region where local superconducting order persists and phase fluctuation scenario applies is much smaller than the observed pseudogap region [Fig. 1.5]. Therefore, phase fluctuations of the pre-formed Cooper pairs alone cannot account for the wide range of the pseudogap phase.

Another viewpoint concerning the nature of pseudogap is based on Landau's symmetry-breaking theory where a competing order is assumed to be responsible for the pseudogap phenomena. In contrast to earlier tunneling spectroscopy with limited spatial resolution that shows smooth transition from the superconducting phase to the pseudogap phase [57, 54], recent spatially resolved scanning tunneling spectroscopy measurements indicate that there are two types of single-particle spectra with different gap values coexisting in the underdoped and optimally doped Bi-2212 samples [67, 68]. Furthermore, the interlayer tunneling spectra of Bi-2212 mesa samples demonstrate that the sharp superconducting coherence peaks coexist with a gradual hump feature at $T \ll T_c$, and that the superconducting gap vanishes above T_c while the higher energy hump background persists till $T^* > T_c$ [69]. The ARPES measurements on $La_{2-x}Sr_xCuO_4$ [70] and the bulk specific heat measurements [71] also support the conjecture of the pseudogap phase as a competing order phase. Candidates for the competing order include (fluctuating) stripe order [72, 73], circulating current order [74] also known as d-density wave order [75], (dynamic) anti-ferromagnetic order [76], and valence-bond-solid order [62]. Determining which orders are present in the superconducting and the pseudogap phases is one of the most important current topics of cuprate physics [62, 58, 73, 76].

In contrast to the ubiquitous presence of pseudogap above T_c in underdoped p-type cuprates [55, 56, 9], *no* discernible normal state single-particle excitation gap has been observed in the zero-field tunneling spectroscopy of n-type one-layer NCCO and PCCO [16, 17, 18], and *no* discernible normal state leading edge gap has been seen within the resolution of ARPES [77]. Nernst measurement on NCCO also exhibits negligible superconducting fluctuations above T_c [65, 78]. Furthermore, scanning

tunneling spectra of infinite-layer SLCO indicate complete absence of any normal state tunneling gap [§5], and the NMR spin-lattice relaxation rate and Knight shift measurements show that there is no normal state spin gap in this compound [79]. Only when a magnetic field exceeding the upper critical field is applied, would a normal state "pseudogap" appear in the tunneling spectra [17, 18]. However, such a "pseudogap" in n-type cuprates only appears below T_c, which apparently contradicts the precursor Cooper pairing scenario.

To explain the absence of the zero-field pseudogap and the field-induced pseudogap in the electron-doped systems, we propose that the strength of the competing order in the n-type cuprates is smaller than the superconducting gap, which is opposite to their counterparts in the p-type cuprates. Only when the superconducting order is suppressed and the competing order enhanced by a large external field would the single-particle spectral gap associated with the competing order be revealed. In Chapter 6, we present a simple model that implements this conjecture in the calculation of the tunneling spectra for both s- and d-wave cuprate superconductors. Numerical simulations based on this model confirm that our conjecture is consistent with the observed spectral characteristics of the infinite-layer SLCO [§6]. Moreover, it can be shown that, by varying the gap ratio of the two competing orders, the appearance of pseudogap phenomena in hole-doped cuprates can be reconciled with the absence of pseudogap in the electron-doped cuprates.

1.2.3 Orders in cuprate superconductors

On way to differentiate between numerous theories of high-temperature superconductivity is to identify the (static or fluctuating) quantum order that each theory prescribes for the pseudogap and the superconducting phases. Experimentally, spin correlations of several cuprate families have been studied in detail by means of inelastic and elastic neutron scattering for comparison with theoretical predictions. One of the most conspicuous features observed in LSCO and YBCO is the presence of incommensurate spin fluctuations, which are static in the underdoped LSCO with doping $0.055 < p < 0.14$ [80, 81, 82], dynamic in LSCO with $p > 0.14$, and dynamic in YBCO throughout the entire superconducting doping range [83]. In Nd-doped LSCO, Bragg peaks related to static

spin and charge orders are revealed with a charge modulation periodicity half of that of the spin modulation [84]. This observation is consistent with the "stripe" picture where the doped holes self-organize into charge stripes that are the anti-phase domain walls between Néel ordered regions [72]. Similar static stripe-like orders are also detected in $La_{1.875}Ba_{0.125}CuO_4$ [85].

In the stripe phenomenology, the incommensurability δ_q of the spin fluctuations is related to the doping level by $\delta_q = p$, exactly what is observed in underdoped LSCO for $0.055 < p < 0.125$[3] [86]. Therefore, it is proposed that the static incommensurate spin density waves in LSCO are spin stripes, even though the corresponding charge Bragg peaks have never been identified (presumably due to the weak intensity). Furthermore, the dynamic incommensurate spin fluctuations that take place beyond 1/8 doping are interpreted as slowly fluctuating stripes. In comparison, earlier neutron scattering results on YBCO do not provide as strong evidence for stripe formation. Most experimental data on YBCO exhibit dynamic spin fluctuations with a more complicated doping-dependent incommensurability [83]. Recently, one-dimensional incommensurate spectral features have been observed in highly ordered underdoped $YBa_2Cu_3O_{6.5}$, in which the spin fluctuations are incommensurate along the {100} axis and commensurate along the {010} direction [87, 88]. The one-dimensional incommensurate scattering is taken as strong evidence of stripe-like modulations in underdoped YBCO. We remark, in passing, that the neutron scattering experiments on electron-doped cuprates show dynamic *commensurate* spin fluctuations [89, 90, 91, 92], in contrast to the incommensurate scattering of hole-doped cuprates.

Other types of orders that appear in some theories of cuprate superconductivity include the *d*-density wave order [75] (or the circulating current order [74]) branded as the hidden order of the pseudogap phase. The orbital currents flowing in the CuO_2 planes break the time-reversal symmetry and produce a *c*-axis moment. This phase should be visible in the neutron scattering experiments if it exists. To date, the only supportive evidence for the static *c*-axis moment comes from a set of experiments on underdoped $YBa_2Cu_3O_{6.6}$ [93, 94]. However, contradictory results have also been reported for highly ordered $YBa_2Cu_3O_{6.5}$ [87, 88]. Whether the dynamic orbital current fluctuations

[3] Beyond the 1/8 doping, the observed incommensurability of LSCO saturates at 0.125.

of the staggered flux state predicted by the $SU(2)$ slave-boson theory exist or not is yet to be verified.

While spin orders couple directly to neutron magnetic moments, charge correlations can only be detected indirectly through neutron scattering of the induced lattice distortion. The ideal probe for static charge orderings of quasi-two-dimensional samples is the scanning tunneling spectroscopy (STS). Low-temperature scanning tunneling spectra taken on highly anisotropic Bi-2212 have revealed a number of interesting phenomena, including a checkerboard-like charge ordering in the vortex core of nearly optimally doped samples [95], dispersive modulations in the local density of states in nearly optimal doped and slightly underdoped samples [96, 97], and non-dispersive incommensurate modulations in heavily underdoped samples [98]. In addition, it is found that above the superconducting transition temperature, four non-dispersive modulation peaks along the anti-nodal direction survive [99]. These results imply the presence of the checkerboard or stripe order in the pseudogap phase and its coexistence with the superconducting order in the vortex core of the superconducting phase. Another cuprate compound that exhibits incommensurate charge density wave order is the highly two-dimensional Na-doped $Ca_2CuO_2Cl_2$ [100]. In the underdoped samples, all tunneling spectra below T_c reveal pseudogap-like density of states without sharp superconducting coherence peaks, similar to those taken on the non-superconducting samples. Thus, it is tempting to attribute the pseudogap spectra to the presence of charge ordering. An alternative interpretation of the density of states modulation is to view it as a manifestation of the bond-ordered states among which the stripe order is a special case [62]. To distinguish between different bond orders of the same periodicity, the phase information of the Fourier-transformed local density of states must be retained and carefully analyzed [101]. To date, no definitive result has been obtained from such analysis [73].

Up to this point, we have only discussed the orders that break explicit symmetries such as the spin-rotational symmetry, the lattice symmetry, or the time-reversal symmetry. There are other theories that conjecture more subtle topological orders as the relevant orders that characterize the pseudogap phase. These theories are based on the RVB scenario [20] that postulates a common origin for the pseudogap and the superconducting phases as a doped spin liquid state. Two types of spin

liquids most discussed in the context of cuprate superconductivity are the Z_2 [102] and $U(1)$ spin liquids [103, 58] characterized by their respective low-energy gauge groups. At the time of writing, the experiments designed to detect the non-trivial fluxes [104] associated with the topological order have not produced any positive result [105, 106]. Therefore, we shall restrict our discussion to the symmetry-breaking orders in this thesis.

1.3 Overview of the thesis

This thesis presents scanning tunneling spectroscopic studies of two families of cuprate superconductors, the hole-doped cuprate YBCO, and the electron-doped cuprate $Sr_{0.9}La_{0.1}CuO_2$ (SLCO). Their contrasting properties, such as the pairing symmetries and pseudogap phenomena, are highlighted, and a proposal to unify these apparent non-universal phenomena in terms of coexisting orders is put forward. The theoretical model based on this proposal is solved by numerical methods, and the results are found to reconcile the findings in the low-energy quasiparticle spectral characteristics of different cuprates.

The thesis is organized as follows. Chapter 2 first describes the fundamental physics of tunneling spectroscopy within the tunneling Hamiltonian formalism. The Blonder-Tinkham-Klapwijk (BTK) theory is then introduced to treat the tunneling spectra of superconducting electrodes with a variable junction barrier [Appendix A]. For superconductors of unconventional pairing symmetries, the generalized BTK theory is derived in order to account for the Andreev bound state developed at the sample surface along the nodal direction. Tunneling spectra of d-wave superconductors along the nodal, anti-nodal, and c-axis are summarized, and comparisons are drawn among the spectra of various mixed pairing symmetry superconductors.

Chapter 3 begins with a brief review of the scanning tunneling microscopy (STM) technique, followed by detailed description for the instrumentation of the cryogenic STM built for the thesis research. The working principle of the STM and the essential components are outlined. The specifications of the STM electronics and the high-voltage circuitry for piezoelectric control are provided, and the cryogenic probe design is illustrated. Additional elements necessary for a fully functional

STM are documented, which include the improvement of thermal response and measures taken for the vibrational, acoustic, and electrical noise reduction.

Chapter 4 presents the STS results on the hole-doped YBCO with a range of doping. The pairing symmetry and the pairing potential are extracted by fitting to the BTK formalism. Predominantly d-wave pairing is found in underdoped and optimally doped pure YBCO, and in overdoped Ca-YBCO a significant s-wave admixture is revealed by STS. In addition, tunneling spectra of optimally doped YBCO with a small concentration of non-magnetic impurities are studied, which exhibit strong suppression of the superconducting gap and a single resonance peak at the impurity site, consistent with the d-wave pairing symmetry around optimal doping. The implication of the doping-dependent pairing symmetry in the context of quantum criticality and the existence of fluctuating competing orders is discussed.

Chapter 5 presents the tunneling spectra of the electron-doped SLCO. In contrast to the predominantly d-wave pairing in hole-doped cuprates, the order parameter of SLCO is found to be momentum-independent with a single-particle excitation gap substantially exceeding the BCS value. Above T_c, the spectral gap closes, indicating the absence of zero-field pseudogap. The single-particle spectral response to the quantum impurities (Zn and Ni) further corroborates the finding of the s-wave pairing in SLCO. Moreover, it is found that the mean-field Bogoliubov quasiparticle based description fails to account for several important spectral characteristics of SLCO: the excess low-energy excitations, the rapid decrease of the spectral gap with increasing temperatures, and the current-induced pseudogap-like features. These observations are in contrast to the applicability of the mean-field BTK theory to YBCO tunneling spectra and can be understood in terms of the presence of strong quantum fluctuations in SLCO that results from its proximity to a quantum critical point. Additional evidence for strong quantum phase fluctuations have been obtained from studies of high-field vortex dynamics [107] in various cuprates and will be discussed and compared with microscopic quasiparticle spectra.

In Chapter 6, a theoretical model for coexisting density waves with superconductivity is investigated by numerical methods. By incorporating quantum phase fluctuations and using realistic band

structures, we find that the resulting quasiparticle spectra exhibit excess low-energy excitations consistent with empirical results [§5.3.1]. Furthermore, by tuning the ratio of the strength of the competing order to that of the superconducting order, the absence of pseudogap in n-type cuprates, the current-induced pseudogap-like spectra in SLCO [§5.3.2], and the general presence of pseudogap phenomena in hole-doped cuprates [§1.2.2] are reproduced. An additional theoretical manifestation of competing orders is also investigated by considering the interference of quasiparticles scattered off pinned density waves, and the numerical results are found to compare favorably with experimental data in Bi-2212 [95, 97, 99]. Finally, we conclude that competing orders are important in understanding the cuprate phenomenology. Further experiments that investigate the varying proximity to quantum criticality of different cuprate superconductors are proposed for future studies.